Deformation Behavior of PP and PP/ZnO Nanocomposites As Studied by SAXS and WAXS

Xiuhong Li,† Konrad Schneider, Bernd Kretzschmar, and Manfred Stamm*

Leibniz-Institut für Polymerforschung Dresden, Hohe Strasse 6, 01069 Dresden, Germany

Received December 20, 2007; Revised Manuscript Received March 28, 2008

ABSTRACT: Structural changes during tensile stretching deformation for pure polypropylene (PP) specimen and PP/ZnO specimens with different content of ZnO nanoparticles have been investigated by small-angle X-ray scattering (SAXS) and wide-angle X-ray scattering (WAXS) techniques. For pure PP specimen, there is a large amount of cavities appearing during stretching. The cavities are first extended in the equatorial direction and then elongated along stretching direction. At high strain some edge dislocations appear in PP lamellae structures. For PP/ZnO specimens, lamellar structures are destroyed gradually during stretching. At low ZnO loading (<0.5%), after stretching to strain of about 500%, the scattering intensity of cavities and dislocations is a little lower than that from pure PP. For the case of high ZnO loading (>0.5%), the scattering intensity of cavities and dislocations increases linearly with ZnO content. WAXS results indicate that, compared with the undeformed specimen, the crystallinity of all specimens shows a little decrease after stretching to about 500% strain.

1. Introduction

Polypropylene (PP) has widespread applications in diverse areas such as household, automotive, and electrical industries. Nanoparticle-strengthened thermoplastics offer much more possibilities.[1] These polymer nanocomposites derive their usefulness and versatility from their improved toughness, heat and chemical resistance, and good mechanical and electrical properties.[2] PP exposure to sunlight and related degradations are important issues to engineering application when it is applicated under outdoor environments.[3] Severe molecular chain degradation in PP can be induced when it is irradiated within the active wavelength range of 310−350 nm,[4] which means that photodegradation can occur easily in PP-based materials. Zhao and co-workers investigated the photodegradation characteristics for ZnO nanoparticle-filled PP nanocomposites.[3] It was observed that UV irradiation induced significant photodegradation for unfilled PP. However, with incorporation of ZnO nanoparticles into the PP matrix, the extent of photodegradation was significantly reduced, which is due to the superior UV light screening effects offered by the ZnO nanoparticles. Kruenate et al. studied the optical properties of PP/ZnO nanocomposites.[2] It was found that the PP/ZnO film had a unique property as it blocked UV while transmitted visible light better than PP/SiO_2. PP is also one of the popular plastics in a micro-electromechanical system. PP is easily modified with blending elastomers and inorganic fillers to obtain higher mechanical performances. At the same time, ZnO is a popular semiconductor material with a high excitonic binding energy. ZnO is also found to be a significantly harder material used to fabricate nanowires and nanotips.[5−7] Huang and co-workers investigated the kneading and mechanical properties of PP with adding ZnO nanopowder.[7] The results showed that nanocomposites with a small amount of nanofiller exhibit significant improvement in wear resistance and mechanical properties. Larger amounts (>5 wt %) of nanofillers in the polymer matrix resulted in less resistance to contact wearing than pure polymer.

Understanding the crystal structure development in PP polymer nanocomposites during deformation is essential in PP material design for practical applications. Up to now, polymer deformation has been extensively studied using several techniques including small-angle X-ray scattering (SAXS) and wide-angle X-ray scattering (WAXS), transmission electron microscopy (TEM), Fourier transform infrared microscopy, and birefringence.[8−24] SAXS as a nondestructive technique can be used to study structural changes that take place on a nanometer scale during the stretching of polymer nanocomposites. WAXS can provide the information on crystallinity, orientation distribution of crystallites, and crystallite size. During deformation, some new crystalline phases may be induced by stretching. Hsiao et al. studied the structural change of a semicrystalline ethylene−propylene copolymer during uniaxial deformation by time-resolved synchrotron small-angle X-ray scattering.[9] It was found that there was strain-induced melting, which began at a relatively low strain and was directionally dependent. At 75% strain, new crystals started to form, which coexisted with the original crystals. Sometimes cavities are found in the specimens during deformation. Men et al. investigated the tensile deformation of poly(1-butene) (P1B) and high-density polyethylene (HDPE) by ultrasmall-angle X-ray scattering.[10] During tensile deformation, the main contribution to the scattering intensity is due to platelike cavities in the case of P1B, while such cavity scattering is rarely observed in the case of HDPE. Zafeiropoulos et al. investigated the deformation of polyamide 6 (PA6) during the insertion of a wedge into the material by synchrotron radiation microfocus small-angle X-ray scattering (SAXS).[11] The results revealed that there are different mechanisms of deformation in the different areas around the crack tip. It shows that the damage area propagates far beyond the visible crack, and inside the damaged zone platelet-shaped voids are formed. Schneider and co-workers studied the cavity in high-density polyethylene copolymer using time-resolved synchrotron X-ray scattering during tensile deformation.[12] Competitive phenomena like crystallite fragmentation and cavity formation were found to occur simultaneously in the phase of lowering load but at different length scales. Void formation occurs mainly during yielding.

Although a lot of research work has been done in the past, the details of the underlying processes of void formation and growth, molecular orientation, and phase transformation during tensile deformation are still poorly understood. Up to now, the effect of ZnO nanoparticles on the PP matrix during stretching has not been investigated. In our case, at a stretching speed of

* To whom correspondence should be addressed. E-mail: Stamm@ipfdd.de.
† Present address: Service de Physique de L\'Etat Condensé, Orme des Merisiers, CEA/SACLAY, F-91191, France.

10.1021/ma702834y CCC: $40.75
Published on Web 05/28/2008

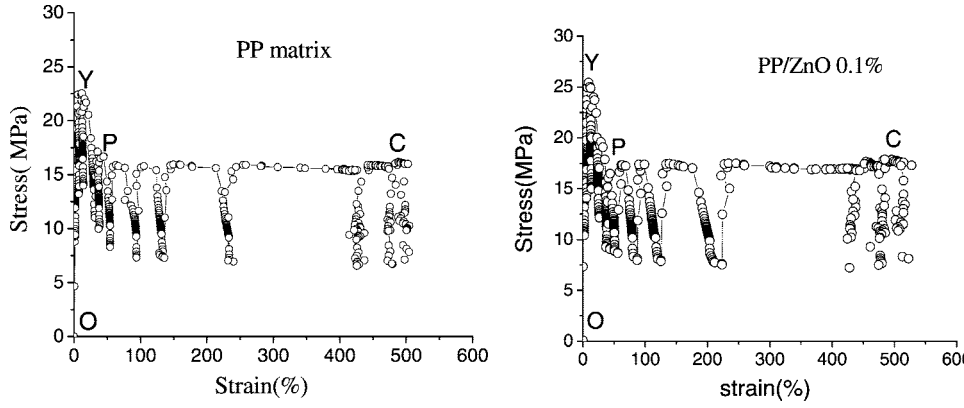

Figure 1. Stress−strain curves of PP and PP/ZnO 0.1% specimens. In the figures, OY represents quasi-elastic zone, YP represents quasi-plastic zone I, and PC represents plastic zone II.

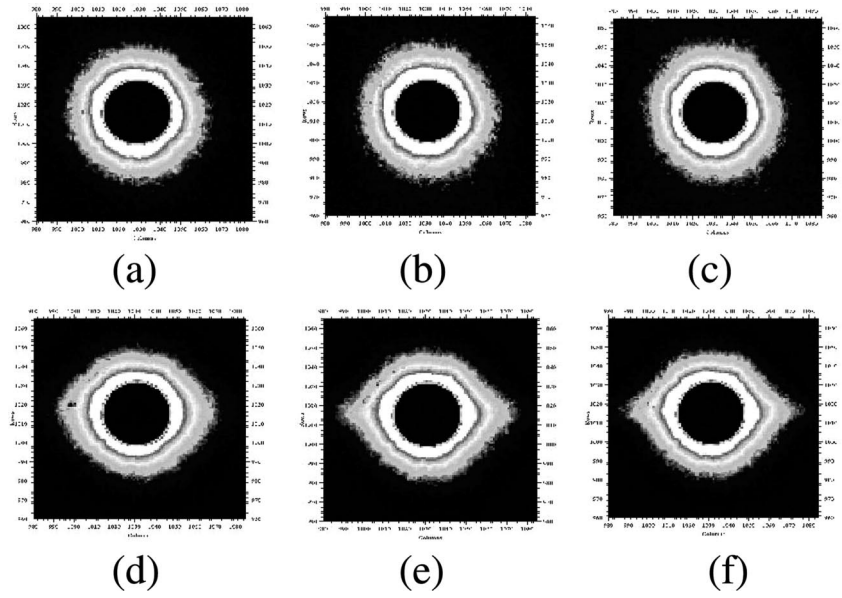

Figure 2. Deformation SAXS patterns of pure PP specimen measured at different strains. Tensile direction is along vertical. (a) 0% strain; (b) 14% strain; (c) 30% strain; (d) 51% strain; (e) 426% strain; (f) 502% strain.

10 mm/min, yield stress of PP mixed with ZnO increase with ZnO content, while elongation at break only decreases very little. After incorporting ZnO nanoparticles, it is expected that we can obtain nanocomposites with improved mechanical properties. In the present study, SAXS and WAXS measurements were carried out to investigate the structural changes for pure PP and PP/ZnO specimens during the deformation. Our study aims at the understanding of the deformation behaviors of the PP matrix and PP/ZnO specimens in order to identify the role of ZnO nanoparticles during stretching deformation.

2. Experimental Section

Isotactic PP is purchased from Borealis, grade HD120MO with a molecular weight of $M_w = 290\,000$ g/mol and the polydispersity $M_w/M_n = 4.4$. The NanoTeK ZnO nanoparticles are from Nanophase. The averaged primary size of ZnO nanoparticles is 60 nm, and the morphology of ZnO nanoparticles is elongated. The compounds were blended in a twin-screw extruder. The extruder diameter is 25 mm. Because a comparable low ZnO content in PP matrix is desired in the specimens, a two-step process via masterbatch was used to get the compounds produced under comparable processing conditions. In the first step a masterbatch with 10 wt % of ZnO nanofiller was made. In this case the PP polymer pellets and the ZnO nanofiller were separately added by gravimetric dosing systems into the hopper of the extruder. In a second extrusion step these masterbatches were diluted to the material combination with the designated filler content. Then the pure PP specimens and PP/ZnO nanocomposites with different content of ZnO nanoparticles (0.1, 0.5, 2.5, and 7.5 wt %) were prepared by injection molding on an Ergotech 100/420-310 (Demag) machine (plate size: 80 mm × 80 mm × 1 mm).

SAXS measurements were performed in transmission geometry using a three-pinhole collimation system equipped with an Osmic multilayer mirror for higher photon flux at smaller beam spot and a Rigaku rotating anode generator (Cu Kα radiation $\lambda = 0.1542$ nm, operating at 4.2 kW with microfilament). For data collection, a Marccd detector with an average pixel size of 78.7 × 78.7 μm^2 was used. All scattering patterns were first radially averaged to obtained the intensity $I(q)$ ($q = 4\pi/\lambda \sin\theta$) and then corrected for background scattering, X-ray absorption, and sample thickness. The radially integrated intensities were obtained for integration in the azimuthal angular range of $0° \le \psi \le 360°$. The equatorial intensities were obtained by integration in the azimuthal angular range of $-10° \le \psi \le 10°$, while the meridional intensities were obtained by integration in the azimuthal angular range of $80° \le \psi \le 100°$ (meridional direction is along the stretching direction). WAXS investigations were carried out by using Cu Kα radiation with an X-ray 4-circle diffractometer P4 (Siemens, Germany) equipped with area detector system Histar/GADDS (Siemens Analytical X-ray instruments, Milwaukee, WI).

In tensile stretching, waist-shaped specimens were used to concentrate the maximum stress and strain in the middle of the sample. The specimens were stretched stepwise by a custom-made tensile machine (based on the device from Kammrath & Weiss) at a stretching speed of 10 μm/s. For each kind of sample, two waist-shaped specimens (with the size of 0.75 mm thickness and 3.3 mm width) were cut from the injection-molded plates for mechanical testing at the same time. The first one was only for mechanical testing to get strain−displacement curve, and the second one was used for stretching experiments on a SAXS machine. The two specimens were from the same position of the two injection molding plates which were produced at the same time. During stretching, all of the conditions (such as displacement for each step, waiting time between two steps) for the two specimens are the same. For the first specimen, a video camera was used to take images of the specimen during the measurements every 10 s in order to perform microdeformation analysis (performed by the ARAMIS software from GOM, Braunschweig). Then, the correlation between displacement and strain can be obtained. Applying the correlation of strain and displacement to the second specimen, we can get the stress−strain curve during stretching in SAXS experiment. The beam spot size was about 0.9 mm in diameter. During the SAXS experiments, the beam position on the specimen was fixed on the center of the deformation region. The width of the specimen was larger than the beam diameter all of the time during stretching. After stretching to the desired displacement, specimens were equilibrated for 10 min before SAXS scanning. For each step, after getting the SAXS 2D pattern, the transmitted intensity and incident intensity were measured. Because the thickness of the undeformated specimen was known, according to the equation $I = I_0 \exp(-\mu t)$ (assuming μ is constant during stretching), the effective thinkness of the specimen at each step during stretching can be gotten. All of the SAXS data were corrected for the background scattering, X-ray absorption, and sample effective thickness.

3. Experimental Results

Figure 1 shows the stress−strain curves for SAXS tensile stretching experiments of PP and PP/ZnO 0.1% specimens. The periodic stress drops that appear on the plots correspond to stress relaxation of the sample during the recording of the SAXS patterns, when stretching was interrupted. It was shown previously that the structure of crystalline domains will not be affected by the interruption process and that the previous deformation state will recover after restretching in the next step.[25] The curves can be divided into three zones: quasi-elastic zone, quasi-plastic zone I, and plastic zone II (as shown in Figure 1).

Figure 2 shows the SAXS 2D patterns for pure PP specimen at different strain. It revealed that SAXS pattern of the undeformed specimen is nearly isotropic. After extension to 51% strain, there is some orientation along the equatorial direction. Figure 3 shows SAXS integrated intensity curves at different strain for the pure PP specimen. The peak at $q = 0.49$ nm^{-1} originates from the PP lamellar structure. With increasing deformation, from 0% to 51% strain, the intensity shows a strong increase in the low q range (0.1 nm^{-1} < q < 0.3 nm^{-1}). Because the scattered intensity is determined by the difference of the electron densities, the strong increase in the integrated intensities can be assumed to be related to the formation of a large amount of cavities during stretching. Stretching to more than 94% strain, the intensity in the low q range almost does not change any more, indicating that no more cavities are formed at this stage. After stretching to larger than 133% strain, it can be found that the slop of the SAXS curve is about −3. The q^{-3} scattering law indicated the presence of a number of edge dislocations arranged as dislocation dipoles (dipoles are defined as two dislocations of opposite sign separated by a distance) in the sample.[26–28] It indicates that at high strain some edge dislocations appear in lamellae structures.

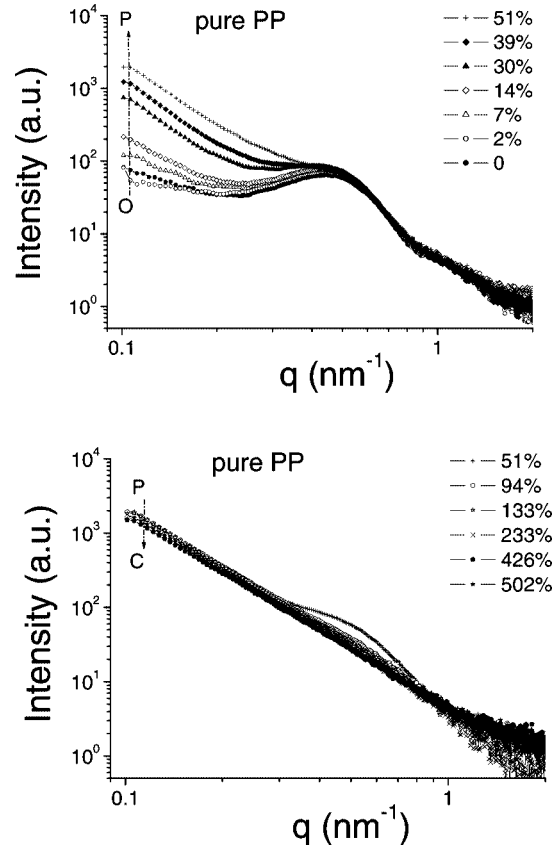

Figure 3. SAXS curves (integrated radially) at indicated strains during stretching of pure PP.

In order to study orientational effects during deformation, the meridional (integration in azimuthal angular range of 80° ≤ ψ ≤ 100°) and equatorial (integration in azimuthal angular range of −10° ≤ ψ ≤ 10°) SAXS scattering curves for pure PP specimen are shown in Figure 4, for quasi-elastic zone (strain from 0 to 14%), quasi-plastic zone I (strain from 14% to 51%), and plastic zone II (strain above 51%). It is evident that structure changes depend on the direction. For the quasi-elastic zone, as shown in Figure 4a,b, the intensities along both directions increase with strain at low q, which can be attributed to small amount of voids appearing. The position and intensity of the lamellar peak in equatorial direction almost do not change. However, in the meridional direction, the position of the lamellar peak shifts to lower q, and the intensity of the lamellar peak increases with strain. The shift of the peak position indicates that the average spacing of the lamellae perpendicular to the stretching direction is enlarged due to the elongation of amorphous chains between lamellae crystals. In quasi-plastic zone I, as shown in Figure 4c,d, the equatorial intensity and the meridional intensity show a strong increase at low q range (0.1 nm^{-1} < q < 0.3 nm^{-1}), which is due to the formation of a large amount of cavities. For lamellar peak intensity, it decreases in meridional direction but increases in equatorial direction, which indicates that some of the lamellar domains are turned into the tensile direction. In addition, the position of the lamellar peak almost does not change in both directions, indicating that the interlayer spacing of the lamellae is not enlarged further in this region. In plastic zone II, as shown in Figure 4e,f, the equatorial intensity is almost constant, while the intensity along meridional direction shows a little decrease.

Figure 5a indicates the change of the meridional and equatorial integrated intensity with strain. In the meridional direction, the intensity first increases (from 0 to 51% strain) and then decreases. The intensity in equatorial direction

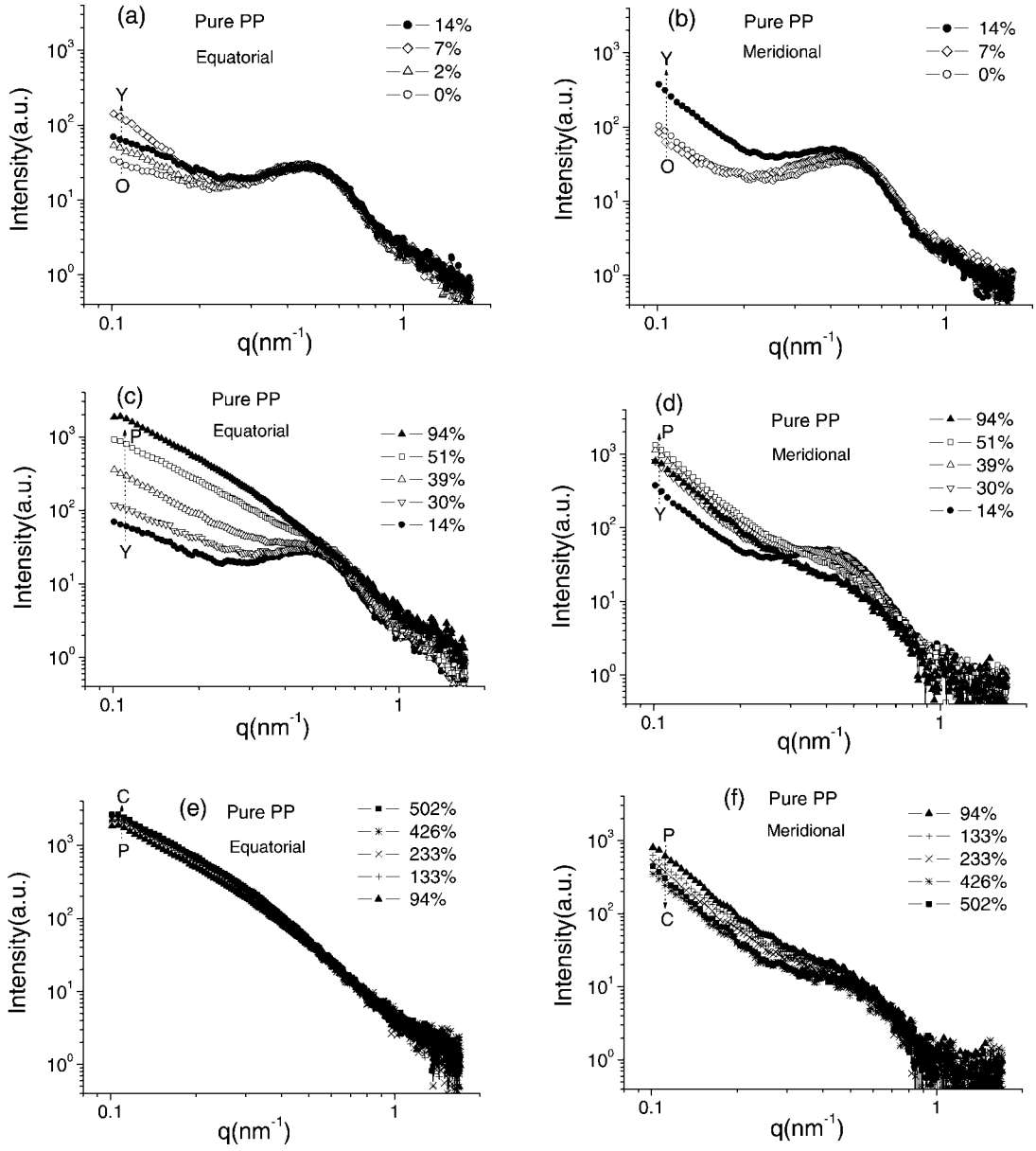

Figure 4. Equatorial and meridional SAXS scattering curves of pure PP at indicated strains (see the Supporting Information for color figures).

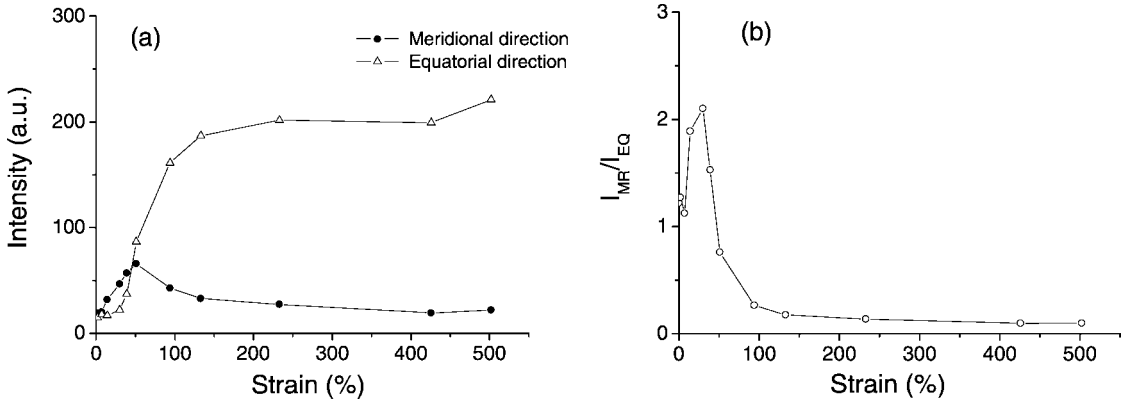

Figure 5. (a) Change of meridional and equatorial integrated intensity with strain for pure PP. (b) Ratio of the meridional and equatorial intensity with strain.

increases gradually until 133%, and after that it is almost constant. Figure 5b shows the ratio of meridional and the equatorial intensity with strain. The change of the ratio can be taken as an indication that the shape of the cavities changes during deformation. When the strain increases from 0 to 39%, the ratio of I_{MR}/I_{EQ} gets larger than 1. It indicates that cavities are first extended in equatorial direction. For strain larger than 51%, I_{MR}/I_{EQ} is less than 1, indicating that cavities are elongated

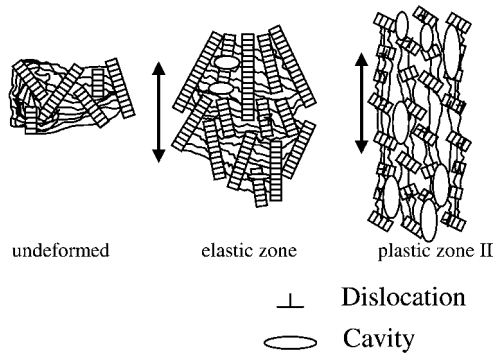

Figure 6. Schematics illustrate the deformation process for the pure PP specimen.

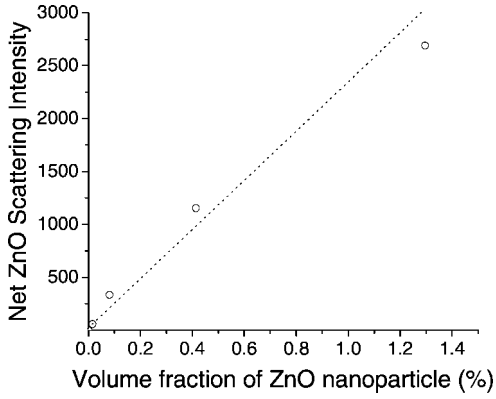

Figure 7. Net ZnO integrated scattering intensity as a function of volume fraction of ZnO nanoparticles in the PP matrix.

in the meridional direction (along stretching direction). Over 133%, there are almost no obvious changes in the ratio of the intensities, showing that the volume fraction of the cavities almost does not change. However, cavities are further stretched along stretching direction. We therefore obtain the following description about the cavities. When the stretching direction is perpendicular to the lamellar normal, cavities are generated within the amorphous phase between the lamellae. Under further stretching, the lamellae are separated by the cavities. At larger strain, the polymer chains along other directions will turn to the stretching direction, and the cavities are elongated along the stretching direction.

According to the experimental results, the deformation process for the pure PP can be described as follows (as illustrated in Figure 6). (1) Quasi-elastic zone: The average spacing of the lamellae is enlarged due to the elongation of amorphous chains between lamellae crystals. Small amount of cavities were formed and cavities were extended in equatorial direction. (2) Quasi-plastic zone I: A large amount of cavities was formed. After strain larger than 51%, cavities are elongated in the meridional direction (along stretching direction). Some of the lamellar domains are turned into the tensile direction. (3) Plastic zone II: Cavities are elongated in the meridional direction (along stretching direction) until 133% strain. After that, the volume fraction of the cavities almost does not change. However, cavities are further stretched along stretching direction. After strain is larger than 133%, some edge dislocation dipoles appeared in the lamellae phase.

In order to study the effect of incorporating ZnO nanoparticles into PP matrix, different amounts of ZnO (0.1, 0.5, 2.5, and 7.5 wt %) in nanocomposites have been investigated. According to the SAXS curves of undeformed pure PP and PP/ZnO 0.1%, 0.5%, 2.5%, 7.5% (shown in Figure 3 and Figure S2, Figure S4 and Figure S5 (in Supporting Information)), the net ZnO scattering intensity for different ZnO content nanocomposites can be obtained. Figure 7 indicates the relationship of the net ZnO integrated scattering intensity with volume fraction of ZnO nanoparticles in PP matrix. It can be seen that the ZnO integrated scattering intensity increase linearly with ZnO content, which indicates that ZnO nanoparticles are homogeneously distributed in the polymer matrix.

Figure 8 shows the SAXS 2D patterns for 0.1% ZnO-reinforced PP specimen. For the undeformed specimen, the intensity is homogenously distributed. With tensile stretching, some orientation along the equatorial direction appears. The meridional and equatorial SAXS scattering intensity profiles of PP/ZnO 0.1% specimen are shown in Figure 9. From SAXS curves, it can be concluded that the change of structure is anisotropic. As shown in Figure 9a,b, the position of the lamellar peak in both directions almost does not change, indicating an uninfluenced interlayer spacing of the lamellae. Only in me-

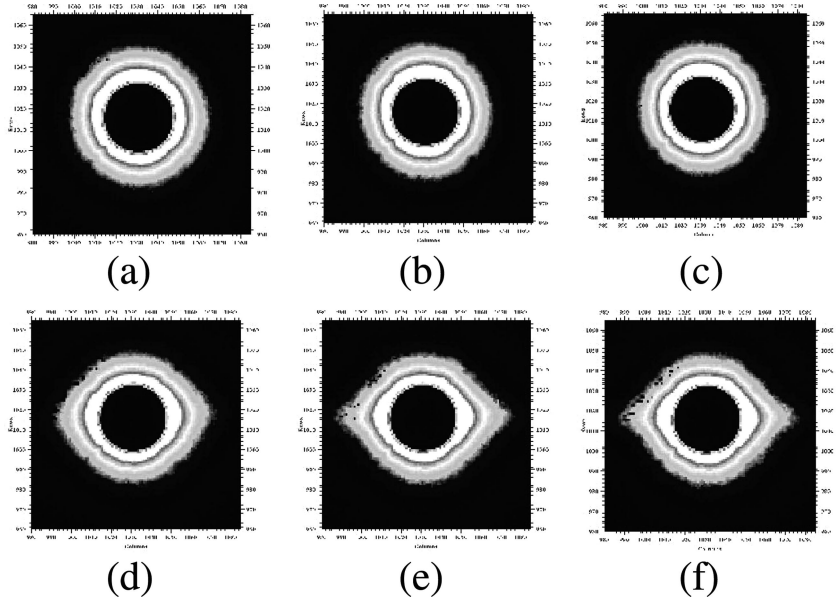

Figure 8. Deformation SAXS patterns of PP/ZnO 0.1% specimen measured at different strains. Tensile direction is along vertical. (a) 0% strain; (b) 14% strain; (c) 26% strain; (d) 51% strain; (e) 431% strain; (f) 514% strain.

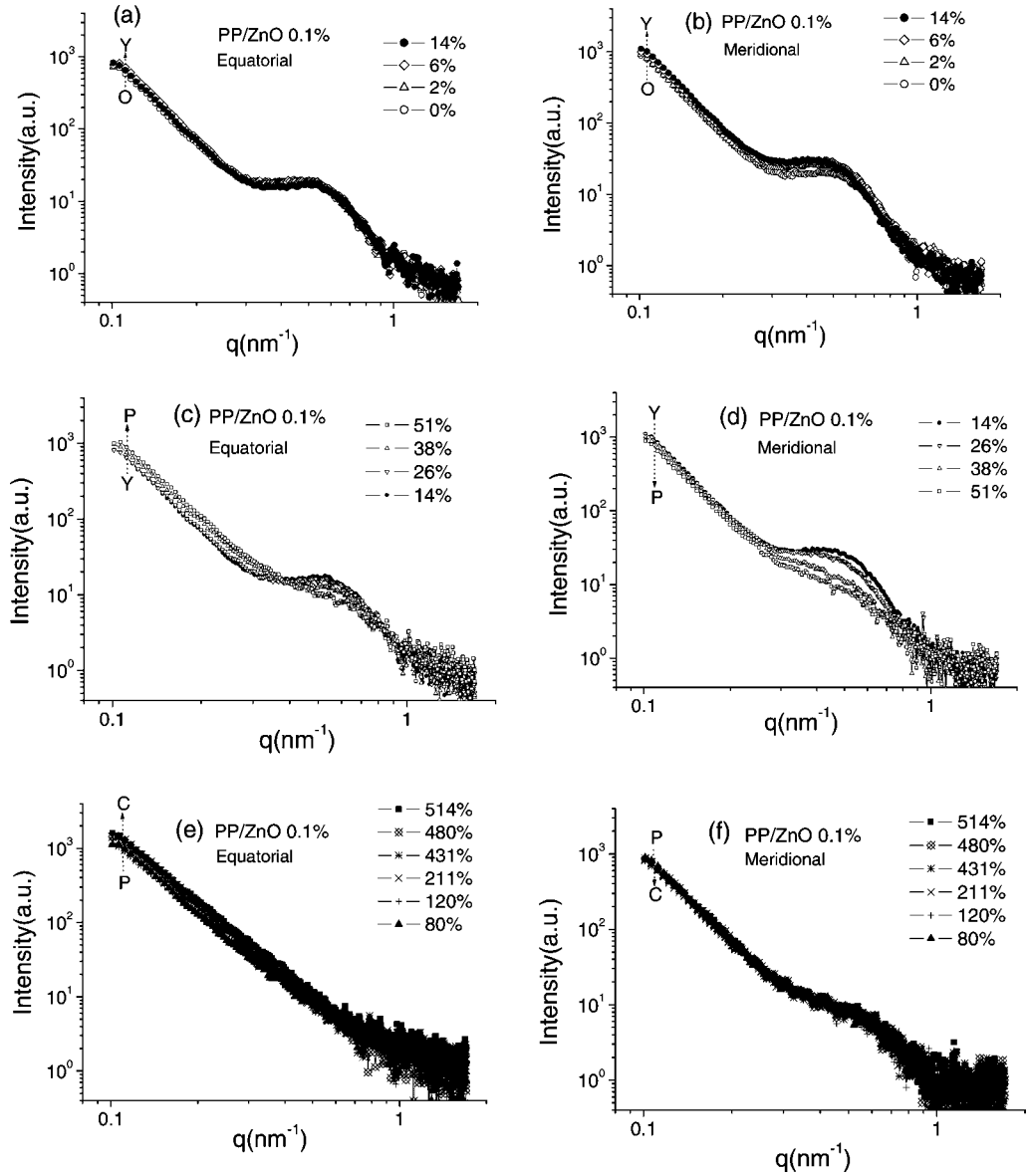

Figure 9. Equatorial and meridional SAXS scattering curves of PP/ZnO 0.1% at indicated strains (see the Supporting Information for color figures).

ridional direction the peak shifts again slightly to lower q values, which can be explained by a widening of the lamellae. In addition, the intensities in the low q range along both directions almost do not change. In quasi-plastic zone I (strain from 14% to 51%), the integrated intensities in the low q range do not increase largely. There is only a slight increase of equatorial intensity. In this zone, the intensities of the lamellar peak in both directions however decrease gradually, while the peak position does not move. The results indicate that after stretching to 14% strain the lamellar phase is destroyed gradually, and the contrast between amorphous and crystalline regions weakens. The destruction process of lamellar structure can be explained as follows. At large strains, the local stress of some extended chains in the amorphous phase will exceed the crystal binding force, resulting in chain pullouts and disintegration of the lamellae, which then become an assembly of smaller lamellar blocks.[9]

In order to investigate the change of the crystalline phase during deformation, WAXS experiments were performed for the specimens before deformation and after extension to about 500% strain. Some of the WAXS patterns are shown in Figure 10. It can be seen that the intensities are isotropically distributed for all undeformed specimens. After extension to about 500% strain, there is some orientation appearing. Figure 11 shows WAXS radially integrated intensity curves for the undeformed specimens and after extension to about 500% strain. Before deformation, PP exhibits α crystalline form for all of the specimens. There is no phase transition due to stretching, but the peaks intensity of α crystalline decrease after stretching to above 500% strain. We take the crystallinity as the ratio of the integral intensities of the crystalline peaks to the total scattering intensity. After separating the intensity from crystalline diffractions and the amorphous component with a curve-fitting program, the crystallinity can be calculated (as shown in Table 1). Compared with the undeformed specimens, the crystallinity shows a little decrease after stretching to about 500% strain.

4. Discussion

From above SAXS analysis it is evident that for pure PP specimen, when strain is larger than 133%, the volume fraction of the cavities almost does not change. Therefore, from the integrated intensities at about 500% strain, we can estimate the maximum scattering intensity of cavities. In order to obtain and

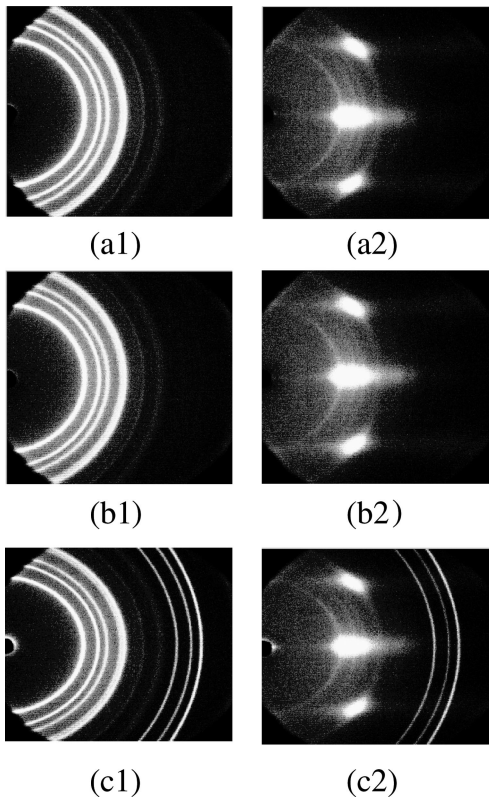

Figure 10. WAXS patterns for the specimens before deformation and after extension to over 500% strain. (a1), (b1), and (c1) are for pure PP, PP/ZnO 0.1%, and PP/ZnO 7.5% specimens before deformation; (a2), (b2), and (c2) are after extension to 502%, 514%, and 529% strain for pure PP, PP/ZnO 0.1%, and PP/ZnO 7.5% specimens, respectively. The stretching direction was along the vertical direction.

compare the maximum scattering intensity of cavities in pure PP, PP/ZnO 0.1%, 0.5%, 2.5%, and 7.5% specimens, the intensity curves at 0% and about 500% strain for all of the specimens (shown in Figure 3 and Figure S2, Figure S4 and Figure S5 (in Supporting Information)) are integrated to obtain total intensities. The total integrated intensities for the specimens are shown in Table 2.

For pure PP, at 0% strain, the SAXS scattering intensity is assumed to originate mostly from the electron density difference between crystalline and amorphous phases; after stretching to about 500% strain, besides the contribution from the crystalline and amorphous phases (here we note it as contribution from PP polymer), the voids and dislocation formed during stretching also contribute to the scattering intensity. For PP/ZnO specimen, at 0% strain, the scattering intensity comes from two parts: one part from PP polymer and another part from ZnO nanoparticles (neglecting correlation contribution); after stretching to about 500% strain, the scattering intensity originates from three parts: one part from PP polymer, the second part from ZnO nanoparticles, and third part from defects (voids and dislocation). Assuming the uniform distribution of nanoparticles and defects (voids and dislocation) in the PP matrix, the cross-terms of the scattering intensity between polymer matrix, nanoparticles, and defects (voids and dislocation) are neglected here. We also assume in this approximation that the electron densities of crystalline and amorphous phases of PP essentially do not change with addition of nanoparticles and during stretching.

From the total intensity of undeformed pure PP specimen, the scattering intensity from the PP polymer then can be directly obtained because there are no other contributions. For pure PP specimen, at about 500% strain, the scattering intensity comes from the PP polymer and the defects (voids and dislocation). During tensile stretching deformation, the scattering intensity from the PP polymer will slightly decrease because the lamellar structure is gradually destroyed and crystallinity decreases. At the same time, the contrast between crystalline and amorphous regions might decrease due to some defects entering into crystalline regions during stretching. But because the scattering intensity from PP polymer is weak and it is decreased, for convenience we can discuss two limiting cases: for the upper

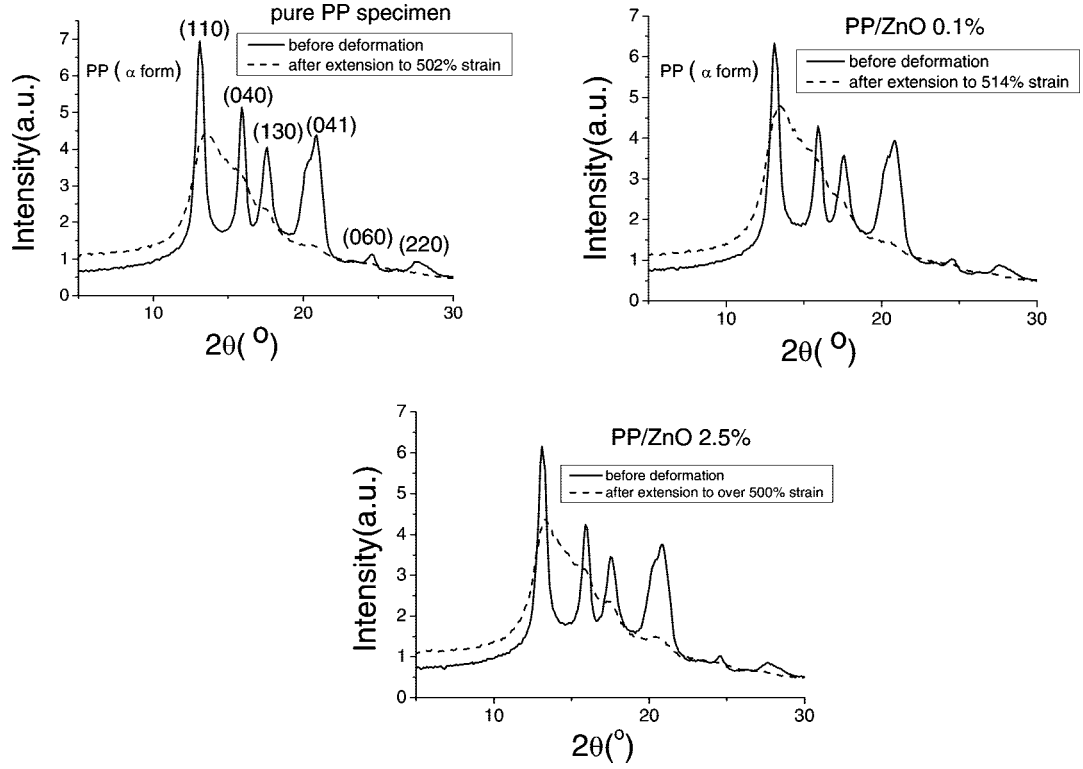

Figure 11. WAXS integrated intensity curves (integration in the azimuthal angular range of $64° \leq \psi \leq 116°$) for the undeformed specimens and after extension to about 500% strain.

Table 1. Crystallinity from the Results of WAXS Investigations

samples	undeformed	after extension to over 500% strain
PP matrix	0.48	0.40
PP/ZnO 0.1%	0.43	0.42
PP/ZnO 0.5%	0.47	0.40
PP/ZnO 2.5%	0.44	0.43
PP/ZnO 7.5%	0.50	0.41

Table 2. Integrated Intensity Contributions from PP Polymer, Nanoparticles and Defects (Voids and Dislocations) at 0% and about 500% Strain for Pure PP, PP/ZnO 0.1%, 0.5%, 2.5%, and 7.5% Specimens

strain	total intensity	intensity from PP matrix	intensity from ZnO nanoparticles	intensity from defects
pure PP at 0%	26.8	26.8		0
pure PP at 502%	117.4	0 − 26.8		90.6 − 117.4
PP/ZnO 0.1% at 0%	83.6	26.79	55.7	0
PP/ZnO 0.1% at 514%	53.1	0	39.7	13.4
PP/ZnO 0.5% at 0%	359	26.78	332.3	0
PP/ZnO 0.5% at 521%	295.99	0	237.3	58.69
PP/ZnO 2.5% at 0%	1179.0	26.69	1152.3	0
PP/ZnO 2.5% at 532%	1187.4	0	823.1	364.3
PP/ZnO 7.5% at 0%	2714.2	26.45	2687.7	0
PP/ZnO 7.5% at 548%	3085.4	0	1919.8	1165.6

limit, it is treated as approximately unchanged, the same as the value in undeformed specimen; for the lower limit, it is treated as 0 (the case that the lamellar structures are totally destroyed). Therefore, after subtracting the contribution from PP polymer, we can get the scattering intensity from the defects (voids and dislocation) for pure PP specimen at about 500% strain.

For undeformed PP/ZnO samples, the total intensity comes from the PP polymer and ZnO nanoparticles scattering. So after subtracting the contribution from PP polymer, the scattering intensity from ZnO nanoparticles can be estimated in first approximation. For PP/ZnO samples after stretching to about 500% strain, the scattering intensity comes from three parts. The first part is from PP polymer. Compared with the scattering intensity from ZnO, scattering intensity from PP polymer is little, and it is decreased with stretching; for convenience we neglect this item and treat as 0. The second part comes from the nanoparticles scattering. According to measurement, the specimen volume (for all deformed part) at about 500% strain is ~1.4 times of the specimen volume (for all deformed part) at 0% strain. It indicates that the number density of the nanoparticles decreases after stretching. Therefore, after sample volume correction, the nanoparticle number in irradiation volume will decrease. Because the scattering intensity of nanoparticles is proportional to number density of the nanoparticles, the scattering intensity from this part will decrease. Assumed that after deformation the nanoparticles are homogenously distributed in the samples, the number density of nanoparticles at about 500% strain becomes about 1/1.4 times of that of undeformed specimen. Then, after considering sample volume correction, the scattering intensity from the nanoparticles at about 500% strain is about 1/1.4 times of the scattering intensity from the nanoparticles at 0% strain. Thus, after subtracting the scattering intensities from the contributions of PP polymer and ZnO nanoparticles, the scattering intensity from defects (voids and dislocations) at about 500% strain can be estimated for PP/ZnO specimens (shown in Table 2).

Figure 12 indicates the obtained scattering intensity from defects (voids and dislocations) as a function of ZnO content. It can be seen that at low ZnO loading (<0.5%) the scattering intensity of defects (voids and dislocations) is a little lower than that from pure PP, while at high ZnO loading the scattering intensity of defects (voids and dislocations) increases linearly with ZnO content.

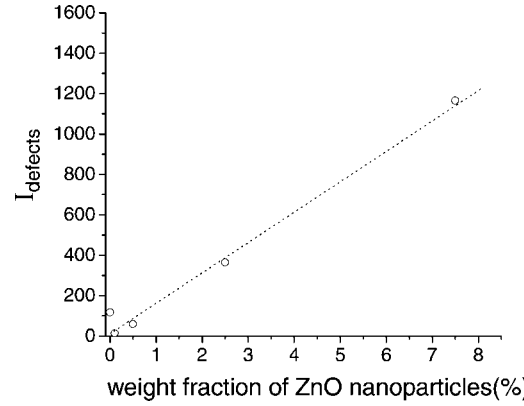

Figure 12. Estimated integrated scattering intensity from defects (voids and dislocations) at about 500% strain as a function of the content of ZnO nanoparticles.

5. Conclusions

The deformation behavior of pure PP and PP/ZnO specimens have been studied by SAXS and WAXS. For pure PP specimen, in the quasi-elastic zone, small amount of voids appears. The average spacing of the lamellar is enlarged. In the quasi-plastic zone I, some of the lamellar structures turned into the tensile direction. A large amount of cavities appear. The cavities are first extended in equatorial direction and then elongated along stretching direction. In plastic zone II, the cavities are further stretched along the stretching direction, while the volume fraction of cavities almost does not change. At the same time, at high strain some edge dislocations appear in lamellae structures. For PP/ZnO specimens, after stretching to strain of about 500%, the scattering intensity of defects (voids and dislocations) increases linearly with ZnO content at high ZnO loading. At low ZnO loading (<0.5%), the intensity of defects (voids and dislocations) is a little lower than that from pure PP.

Acknowledgment. The authors thank Torsten Hofmann for his kind help during SAXS measurements, Dr. Dieter Jehnichen for his support in WAXS measurements, Dr. Sondes Trabelsi for the software instructions, and Dr. Nikolaos Zafeiropoulos for his helpful advice.

Supporting Information Available: Equatorial and meridional SAXS scattering curves (in color) of pure PP; SAXS curves (in color) during stretching of PP/ZnO 0.1% specimen; SAXS intensity curves during stretching of PP/ZnO 0.5%, 2.5%, and 7.5% specimens. This material is available free of charge via the Internet at http://pubs.acs.org.

References and Notes

(1) Garcia Curiel, M. M. L. Polymer-Inorganic Nanocomposites. Thesis, University of Twente, Enschede, The Netherlands, 2004.
(2) Kruenate, J.; Tongpool, R.; Panyathanmaporn, T.; Kongrat, P. *Surf. Interface Anal.* **2004**, *36*, 1044.
(3) Zhao, H.; Li, R. K. Y. *Polymer* **2006**, *47*, 3207.
(4) Allen, N. S.; Edge M. *Fundamentals of Polymer Degradation and Stabilization*; Elsevier Applied Science: London, 1992.
(5) Muthukumar, S.; Sheng, H.; Zhong, J.; Zhang, Z.; Emnetoglu, N. W.; Lu, Y. *IEEE Trans. Nanotechnol.* **2003**, *2*, 50.
(6) Park, W. I.; Kim, D. H.; Jung, S. W.; Yi, G. *Appl. Phys. Lett.* **2002**, *80*, 4232.
(7) Huang, C. K.; Chen, S. W.; Wei, W. C. J. *J. Appl. Polym. Sci.* **2006**, *102*, 6009.
(8) Geil, P. H. *Polymer Single Crystal*; Wiley: New York, 1963.
(9) Liu, L. Z.; Hsiao, B. S.; Fu, B. X.; Ran, S.; Toki, S.; Chu, B.; Tsou, A. H.; Agarwal, P. K. *Macromolecules* **2003**, *36*, 1920.
(10) Men, Y.; Rieger, J.; Homeyer, J. *Macromolecules* **2004**, *37*, 9481.
(11) Zafeiropoulos, N. E.; Davies, R. J.; Roth, S. V.; Burghammer, M.;

Schneider, K.; Riekel, Ch.; Stamm, M. *Macromol. Rapid Commun.* **2005**, *26*, 1547.
(12) Schneider, K.; Trabelsi, S.; Zafeiropoulos, N. E.; Davies, R. J.; Riekel, Ch.; Stamm, M. *Macromol. Symp.* **2006**, *236*, 241.
(13) Kawakami, D.; Hsiao, B. S.; Burger, C.; Ran, S.; Avila-Orta, C.; Sics, I.; Kikutani, T.; Jacob, K. I.; Chu, B. *Macromolecules* **2005**, *38*, 91.
(14) Maier, G.; Wallner, G.; Lang, R. W.; Fratzl, P. *Macromolecules* **2005**, *38*, 6099.
(15) Muramatsu, S.; Lando, J. B. *Macromolecules* **1998**, *31*, 1866.
(16) Wang, K. H.; Chung, I. J.; Jang, M. C.; Keum, J. K.; Song, K. H. *Macromolecules* **2002**, *35*, 5529.
(17) Zafeiropoulos, N. E.; Davies, R. J.; Schneider, K.; Burghammer, M.; Riekel, Ch.; Stamm, M. *Macromol. Rapid Commun.* **2006**, *27*, 1689.
(18) Jar, P. Y. B.; Creagh, D. C.; Konishi, K.; Shinmura, T. *J. Appl. Polym. Sci.* **2002**, *85*, 17.
(19) Ferreiro, V.; Coulon, G. *J. Polym. Sci.* **2004**, *42*, 687.
(20) Choi, D.; White, J. L. *Polym. Eng. Sci.* **2002**, *42*, 1642.
(21) Fleischmann, E.; Koppelmann, J. *Kunststoffe* **1987**, *77*, 405.
(22) Fleischmann, E.; Koppelmann, J. *Kunststoffe* **1988**, *78*, 453.
(23) Lamberti, G.; La Carrubba, V.; Piccarolo, S.; Brucato, V. *Polym. Bull. (Berlin)* **2003**, *50*, 413.
(24) Lamberti, G.; Peters, G. W. M.; Schrauwen, B. A. G. *Polym. Bull. (Berlin)* **2003**, *50*, 405.
(25) Hong, K.; Rastogi, A.; Strobl, G. *Macromolecules* **2004**, *37*, 10165.
(26) Long, G. G.; Levine, L. E. *Acta Crystallogr.* **2005**, *A61*, 557.
(27) Seeger, A. K. *J. Appl. Phys.* **1959**, *30*, 629.
(28) Heuser, B. J.; Allain, M M. C.; Chen, W. C. *Phys. Rev. B* **2002**, *66*, 155419.

MA702834Y